2004

Single-sided CZT strip detectors

John R. Macri
University of New Hampshire - Main Campus, John.Macri@unh.edu

L A. Hamel
University of Montreal

Manuel Julien
University of Montreal

R S. Miller
University of New Hampshire - Main Campus

B Donmez
University of New Hampshire - Main Campus

See next page for additional authors

Recommended Citation
Macri, J.R.; Hamel, L.-A.; Julien, M.; Miller, R.S.; Donmez, B.; McConnell, M.L.; Ryan, J.M.; Widholm, M., "Single-sided CZT strip detectors," Nuclear Science, IEEE Transactions on , vol.51, no.5, pp.2453,2460, Oct. 2004

Single-Sided CZT Strip Detectors

John R. Macri, *Member, IEEE*, Louis-Andre Hamel, Manuel Julien, Richard S. Miller, Burçin Dönmez, Mark L. McConnell, James M. Ryan, and Mark Widholm

***Abstract*—We report progress in the study of thick CZT strip detectors for 3-D imaging and spectroscopy and discuss two approaches to device design. Unlike double-sided strip detectors, these devices feature both row and column contacts implemented on the anode surface. This electron-only approach circumvents problems associated with poor hole transport in CZT that normally limit the thickness and energy range of double-sided strip detectors. The work includes laboratory and simulation studies aimed at developing compact, efficient, detector modules for 0.05 to 1 MeV gamma radiation measurements while minimizing the number and complexity of the electronic readout channels. These devices can achieve similar performance to pixel detectors for both 3-D imaging and spectroscopy. The low channel count approach can significantly reduce the complexity and power requirements of the readout electronics. This is particularly important in applications requiring large area detector arrays. We show two single-sided strip detector concepts. One, previously reported, features rows established with collecting contacts and columns with noncollecting contacts. Another, introduced here, operates on a charge sharing principle and establishes both rows and columns with collecting contacts on the anode surface. In previous work using the earlier strip detector concept we reported simulations and measurements of energy and spatial resolution for prototype 5- and 10-mm-thick CZT detectors. We now present the results of detection efficiency and uniformity measurements conducted on 5-mm-thick detectors using a specific configuration of the front-end electronics and event trigger. We discuss the importance of the detector fabrication processes when implementing this approach.**

***Index Terms*—CdZnTe, CZT, gamma-ray, strip detectors.**

I. Two Single-Sided Strip Detector Concepts

Figs. 1 and 2 illustrate the anode patterns for two approaches to single-sided strip detector design. Note that the guard ring electrode surrounding these anode patterns and the cathode contacts on the opposite sides are not shown.

The first single-sided strip detector concept and its construction were described previously [1], [2]. Fig. 1 illustrates the anode contact pattern. The 8 row × 8 column pattern forms 64 1-mm^2 unit cells. There is a 200-μm-diameter pixel contact pad at the center of each unit cell. The metallic contacts are shown in gray and black. Gaps between contact electrodes are 200 μm, A signal from each interconnected pixel row provides the event trigger as well as the energy and y coordinate. A signal from each orthogonal strip, biased between cathode and pixel row potentials, provides the x and z coordinates. For optimum performance, this approach requires that the orthogonal strip contacts collect no charge but register the motions of electrons as they are collected on the pixels.

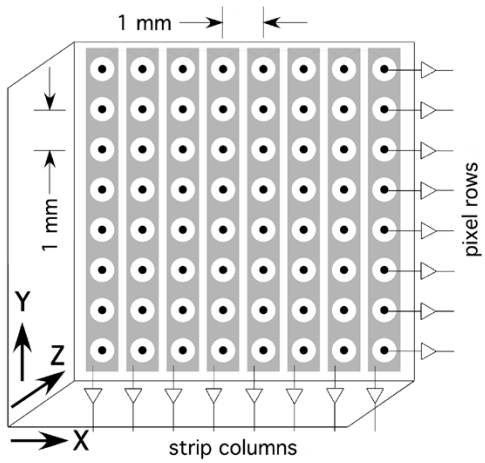

Fig. 1. Single-sided strip detector with collecting (row) and noncollecting (column) contacts on the anode surface.

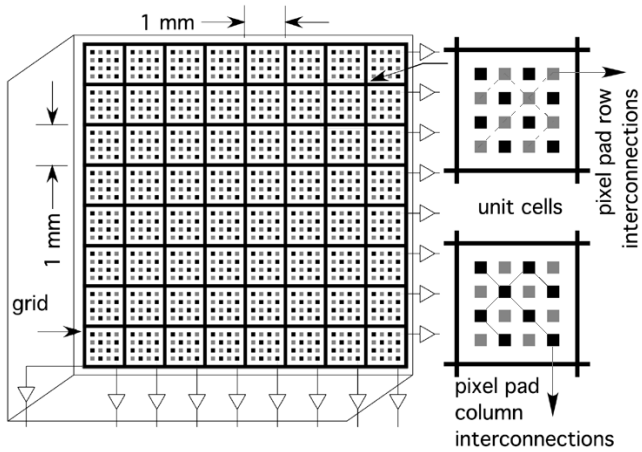

Fig. 2. Single-sided charge-sharing strip detector (left). Unit cells (right) show interconnections.

The second concept is a single-sided charge-sharing strip detector. Fig. 2 shows the anode pattern and two 1-mm unit cells (expanded, right) to illustrate pad interconnections. Unit cells contain an array of closely packed anode contact pads in two groups (gray and black in this illustration). The two groups are identically biased for charge collection but are interconnected

Manuscript received November 14, 2003; revised June 9, 2004, and July 14, 2004. This work was supported in part by NASA's High Energy Astrophysics Supporting Research and Technology Program under Grant NAG5-5327 and by the Natural Sciences and Engineering Research Council of Canada.

J. R. Macri, B. Dönmez, M. L. McConnell, J. M. Ryan, and M. Widholm are with the University of New Hampshire Space Science Center, Durham, NH 03824, USA (e-mail: john.macri@unh.edu; bdonmez@cisunix.unh.edu; mark.mcconnell@unh.edu; james.ryan@unh.edu; mark.widholm@unh.edu).

L.-A. Hamel and M. Julien are with the Department of Physics, University of Montreal, Montreal, QC H3T 1J4, Canada (e-mail: hamel@lps.umontreal.ca; julienman@yahoo.fr).

R. S. Miller is with the University of Alabama in Huntsville, Huntsville, AL 35899 USA (e-mail: millerr@email.uah.edu).

Digital Object Identifier 10.1109/TNS.2004.836091

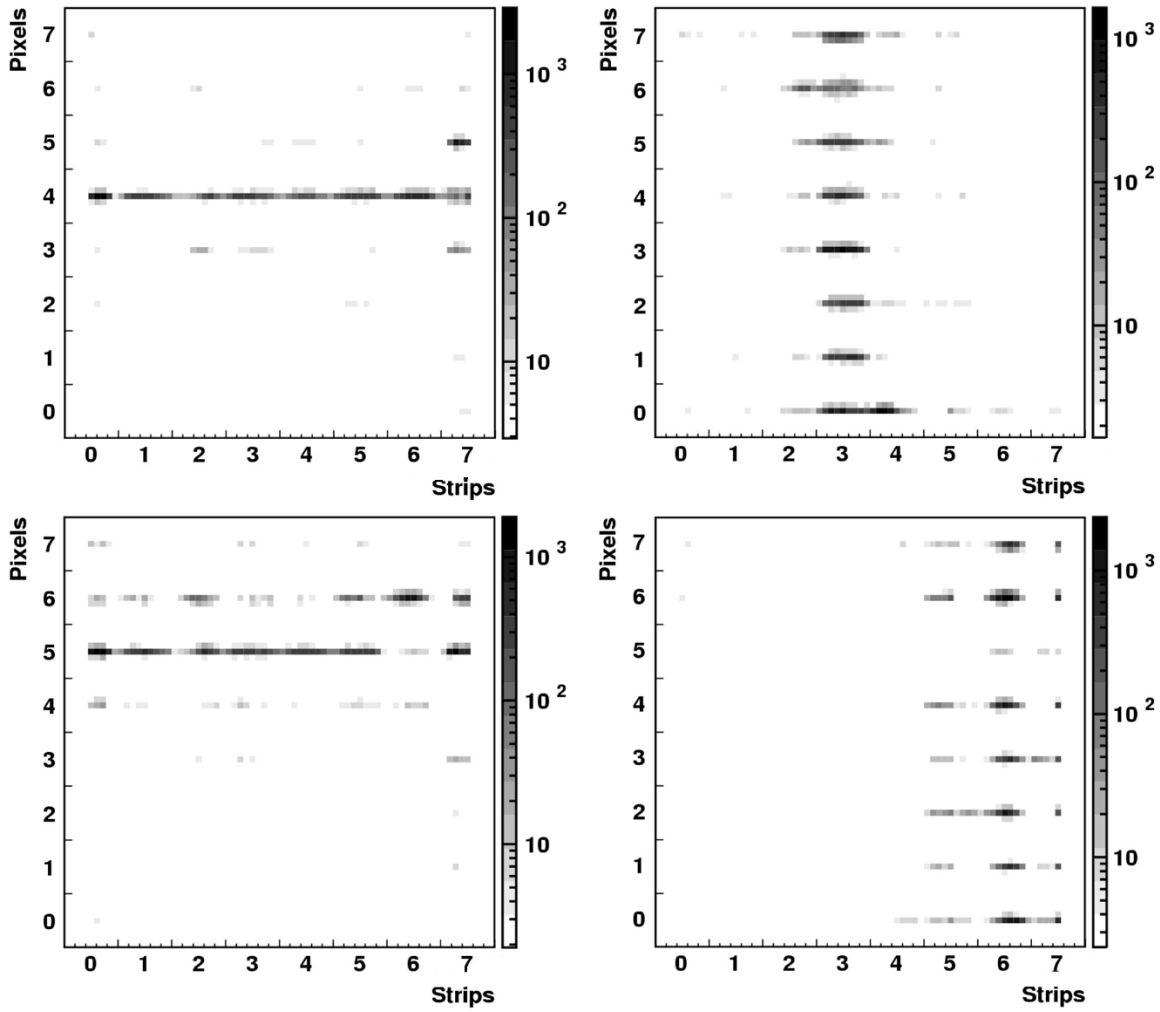

Fig. 3. Reconstructed images at four slit collimator locations. Top panels illustrate relatively uniform image response. Lower panels illustrate a region of nonuniform image response (strip column 6, pixel row 5).

in columns or rows in the layers of the carrier substrate. A noncollecting grid electrode, biased between pixel pad and cathode potentials, provides a signal that can be used for measuring the depth of interaction, the z coordinate. The principle of operation requires sharing of the electron charge between row and column electrodes for each event. This is feasible when the lateral extent of the electron cloud exceeds the pitch of the anode pads. This approach takes advantage of the increasing capability of manufacturers to interconnect fine features of anode contact patterns with the carrier substrates. Interconnections, shown schematically in the both figures, are implemented on the layers of the carrier substrates.

II. Status

Prototype devices employing the first approach (Fig. 1) have been built and tested. Spectroscopy, imaging and relative efficiency results for several devices were reported previously [1], [3]. Energy resolution (FWHM) at 60, 122, and 662 keV as good as 6%, 3%, and 1%, respectively and submillimeter position resolution in three dimensions down to 60 keV have been demonstrated with 5-mm-thick detectors. We have also demonstrated relative detection efficiencies as expected throughout the detector thickness. Significant variations in performance, however, have been observed between detector samples and within the active volumes of individual detectors. New measurements assessing detection efficiency and uniformity of response are reported below. Prototypes employing the new approach (Fig. 2) are in the design phase.

III. Uniformity and Efficiency Measurements

A single detector, ID UNH-EV-3, was selected for the laboratory studies reported in this section. This 5-mm-thick detector, procured in 1999, was chosen from among the early prototype devices for its relatively uniform spectroscopic and imaging performance [3].

Any of the 8-pixel-row signals exceeding its independent discriminator's threshold triggers acquisition of 19 pulse heights (8 pixel rows, 8 strip columns, cathode, guard ring, and strip sum) for the event. A shaping time of 1 μs is used except for the strip column signals where a faster (200 ns) shaping helps to extract the signal used to measure the x coordinate. We studied the imaging and triggering uniformity of this detector by scanning the entire cathode surface in 0.5-mm steps with collimated

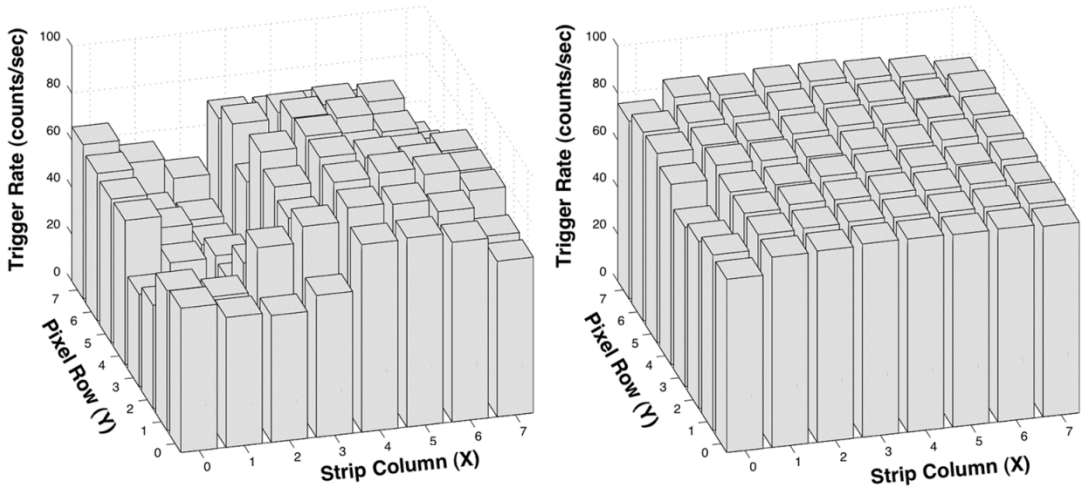

(a) (b)

Fig. 4. Trigger rate maps from scan of 8 × 8 mm imaging region with 1-mm-diameter beam spot from collimated ^{57}Co source (a) using pixel row trigger and (b) using cathode trigger.

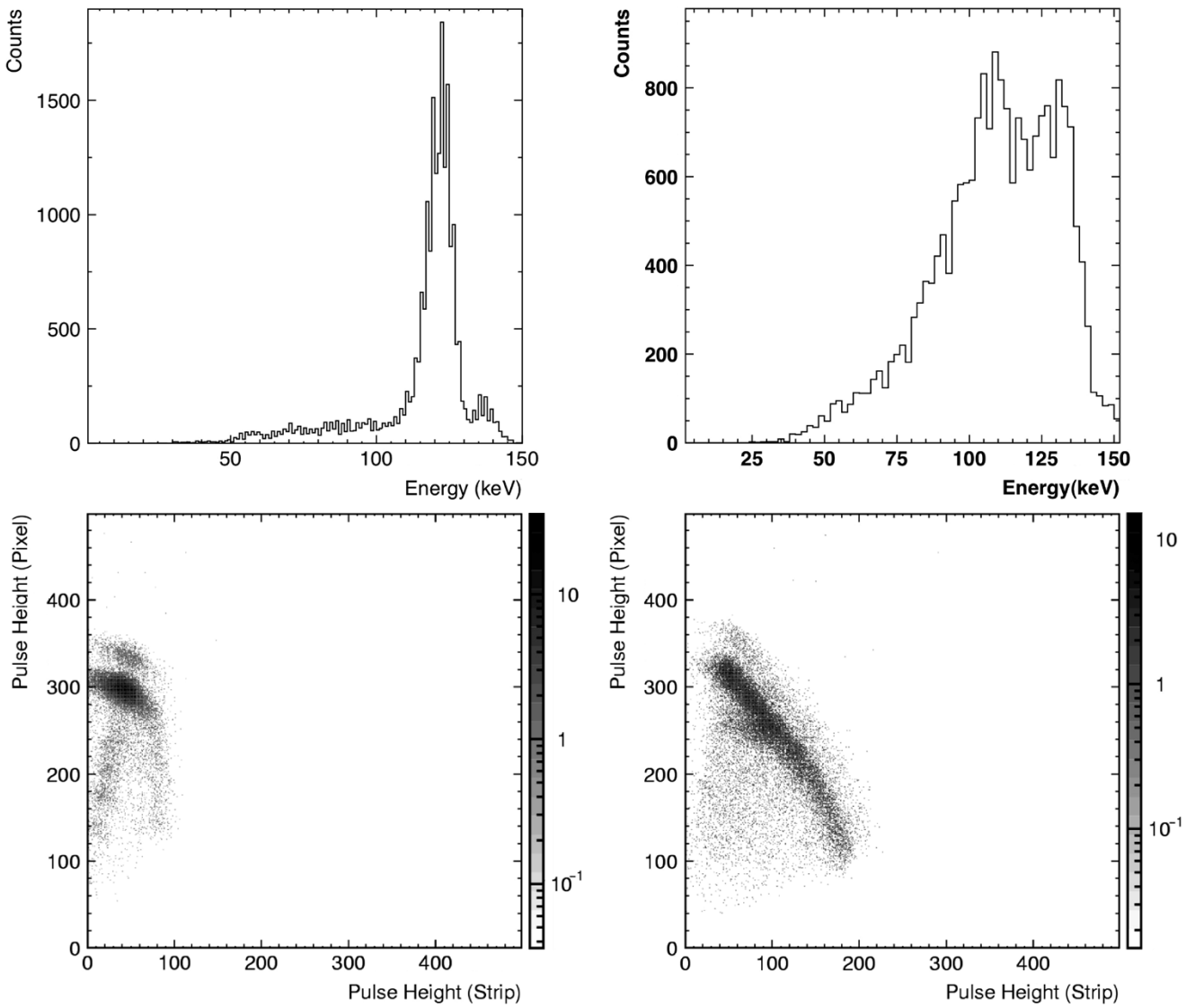

Fig. 5. Spectra (top) and scatter plots of strip column (x-axis) vs. pixel row (y-axis) pulse height (bottom) for two ^{57}Co spot collimator locations (x, y): (3, 4) left; (1, 6) right.

photons from a ^{57}Co source. Both a 1-mm-wide slit collimator and a 1-mm-diameter beam spot collimator were employed. We determined in an independent measurement using a 1.5-in-thick NaI(Tl) detector that ~82 photons/s (122 and 136 keV) are incident on the detector through the spot collimator. The pixel row trigger level was set at ~60 keV.

Rows and columns in our 8 × 8 prototype detectors are numbered 0 through 7. Event locations computed using interpolation of the recorded pulse heights, are shown for four orientations and positions of the slit collimator (Fig. 3). The y position is more quantized than the x position because, unlike for the column electrodes, there is very little charge sharing among adjacent pixel rows with this design. Relatively uniform images of the slit are obtained for most collimator locations such as those shown in the upper panels. The lower panels, however, reveal a region at strip column 6, pixel row 5 where photons, while detected, are registered in adjacent locations. This is the only "pixel" or row–column intersection of the 64 "pixel" imaging region for which the event locations are in error by more than 1 mm.

The spot collimator was used to scan the 8 × 8 mm imaging region. A map of the measured trigger rate for each spot location is shown in Fig. 4(a). The average trigger rate from the source, 65/s, is less than expected (~82/s). It varies by 136% peak to peak, 28% $(1-\sigma)$. A pronounced dip in the trigger rate can be seen along strip column 1 [Fig. 4(a)]. The maximum trigger rate measured, 99/s, corresponds to strip column 3, pixel row 4.

To help identify the sources of trigger nonuniformity, we made a similar scan with the spot collimator (1-mm steps) using the cathode signal to provide the trigger. The response is much more uniform [Fig. 4(b)]. The average trigger rate, 81/s, is consistent with expectations. It varies by 20% peak-to-peak, 4% $(1-\sigma)$. This indicates that anode contact nonuniformity and mismatches of the pixel row trigger channels are more likely sources of this nonuniformity than is the bulk material.

Spectroscopic analysis of the beam spot data was employed to help identify one source of response nonuniformity—strip column charge collection. Fig. 5 shows spectra (top) and scatter plots (bottom) of strip column (x axis) versus pixel row (y axis) pulse height for two positions of the ^{57}Co spot collimator.

The best spectral performance is achieved for photons incident on strip column 3, pixel row 4 (left). Note that this is the location where the maximum trigger rate was registered in the beam spot scan (Fig. 4, left). The worst spectrum is seen for photons incident at strip column 1, pixel row 6 (right). This is the location of the depression in the trigger rate map (Fig. 4, left). To assess the extent of strip column charge collection in these cases the strip column signals were processed using the same shaping and polarity as is used for the pixel rows. The scatter plot (lower right) confirms that the low measurement of energy for most events is the result of a significant portion of the ionization charge being collected on the "noncollecting" strip column electrode in this region. The effect is independent of the depth of interaction (z). We feel it is the result of inadequate control and nonuniform application of the surface preparation, patterning, and bonding processes.

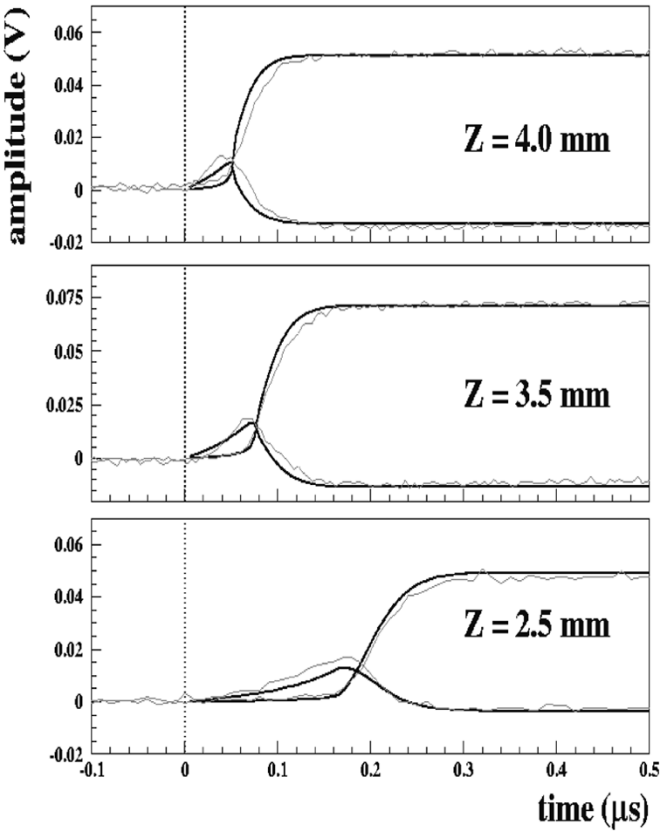

Fig. 6. Measured and simulated pixel row and strip column signals at various depths of interaction. The strip column signals are smaller and bipolar in nature.

IV. Signal-Processing Requirements

Charge collection on the strip columns is a significant factor in reducing the level of the pixel row trigger signal. Nonuniformity of charge collection further complicates the situation. Charge collection on the strip columns also affects the ability to measure the x coordinate of the interaction.

Pixel row and strip column signals (relative units) are shown for various interaction depths in Fig. 6. Even with effective noncollecting electrodes, the smaller, bipolar, strip column signals present the most challenging set of front-end electronics requirements. These smaller signals, typically 25% of the collecting signals, effectively define the lower energy threshold by limiting the ability to measure the x coordinate of the interaction.

A shaping time of 200 ns was selected to process the strip column signals. This selection is effective in measuring a feature of these signals that is common for interactions at any depth, the falling edge that occurs when electrons are collected on the nearest pixel contact. Any charge collection on the strip columns reduces this component of the signal thus limiting the ability to measure the x coordinate of the interaction. Nonuniformity of charge collection on strip columns across the detector increases the difficulty when applying this technique. Another consideration is the difficulty associated with finding or developing a low-noise, low-power front-end ASIC with 200 ns shaping constant.

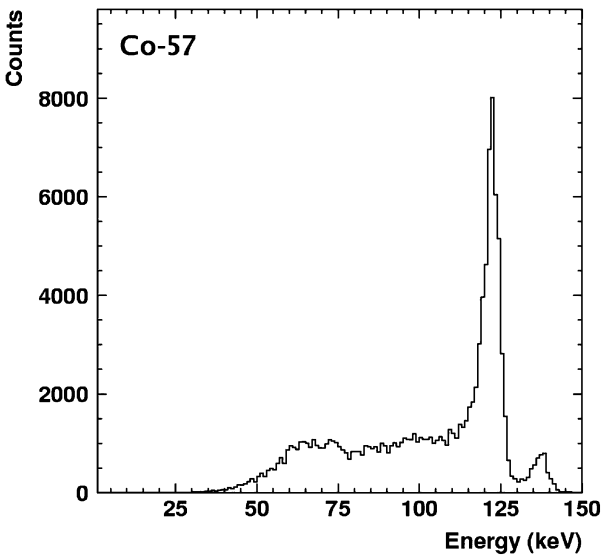

Fig. 7. Composite ^{57}Co spectrum of all 64 "pixels" of a recently procured prototype detector.

V. Improved Fabrication and Performance

Two new 5-mm-thick prototype detectors with this anode pattern have been recently evaluated. These detectors were fabricated using eV Products' coplanar grid (CPG) materials and processes. CPG spectrometer detectors, like the imaging detectors discussed here, in order to perform well, require both collecting and *effective* noncollecting contacts on the anode surface [4].

The first test results are encouraging and indicate significantly less charge collection on the "noncollecting" electrodes. A spectrum from flood illumination of detector UNH-EV-14 with photons from a ^{57}Co source is shown in Fig. 7. Note that this is a composite spectrum of all 64 "pixels" of the detector without any event selection or correction for interaction depth. The measured energy resolution (FWHM) at 122 keV is 6.8 keV. This is the most uniform spectral response we have recorded to date with one of these detectors. Further tests will evaluate the 3-D imaging and detection efficiency capabilities as well as response uniformity.

The goal with these new prototypes was to identify a controlled process that we can use to further develop this and other single-sided strip detector designs with increased confidence. The capability to fabricate significantly more uniform devices having effective noncollecting electrodes was an important step. The new design discussed below was largely motivated by a desire for a simplified set of signal-processing requirements for the front-end electronics.

VI. Charge-Sharing Strip Detector Design

A. Advantages and Disadvantages

The single-sided charge-sharing strip detector design (Fig. 2) addresses some of the limitations encountered with the earlier design (Fig. 1). The front-end electronics implementation is simplified, particularly with respect to processing the bipolar strip column signals (Fig. 6) from the earlier design. Unlike the previous design, charge collecting signals are used for the x as well as the y coordinate measurement. Polarities and shaping times can be the same for column and row channels. While both column and row signals will be reduced on average to half the total collected charge, the size of the noncollecting strip column signal in the previous design was only one fourth the size and required faster and noisier circuitry. In addition, the large area covered by the grid electrode results in greater depth dependence of the noncollecting grid signal than was available from the individual strip column electrodes in the earlier design. See the simulation section below.

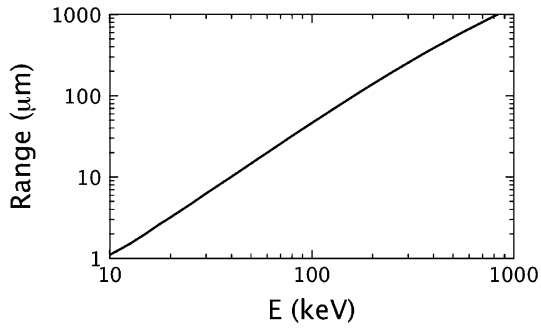

Fig. 8. Electron range in CZT.

There are disadvantages as well. In this new design, column and row signals must be added to measure the energy. This will degrade the achievable energy resolution by a factor related to the electronic noise on each channel. The capacitance between the x and y strips due the compact pad and interconnect structure will also increase the noise. We anticipate, however, that the flexibility afforded to ASIC selection will result in minimal impact here. We anticipate, however, that limited charge sharing due to the small size of the electron cloud at low energies will, for some events, result in the measurement of only one of the two lateral components and will, at least for the first prototype detectors, be a stronger determinant of the effective threshold than the signal size itself.

B. Size of the Charge Cloud

The size of the electron cloud reaching the anode for any given interaction depends on the type of interaction, the energy of the photoelectron or Compton electron, the depth of interaction, and the electric field [5]. The range of a photoelectron in CZT is shown in Fig. 8, [6]. These values represent optimistic estimates of the extent of the electron cloud, as ionization charges are not uniformly distributed along this range. Further study is required to better understand the extent of the charge distribution. Diffusion of the charge cloud as it moves toward the anode surface will help. The rms radius of the carrier distribution increases as $\sqrt{\text{time}}$; thus the actual size of the charge cloud at the collection plane increases as $\sqrt{\text{depth}}$ where the *depth* is measured from the anode. At a bias of 1000 V over a 1-cm-thick detector, charge concentrated at a point will spread, due to diffusion alone, to a radius of 100 μm when the interaction occurs at the cathode. Lower energy photons will interact nearer the cathode surface somewhat compensating for the small initial extent of the charge cloud. The K X-ray produced in photoelectric events will also increase the extent of the charge distribution, particularly at lower energies. Its mean free path is 85 μm.

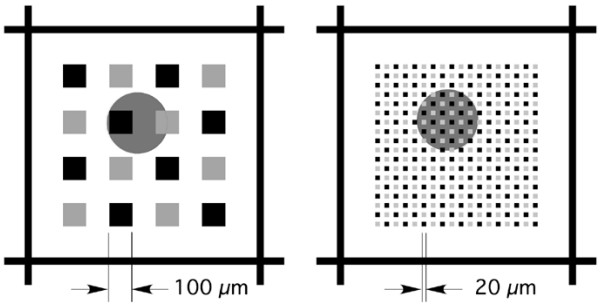

Fig. 9. Unit cells of two charge-sharing strip detectors with a 250-μm-diameter charge cloud projected on the anode. (a) Currently reasonable feature size. (b) Manufacturing goal.

The effective threshold for having sufficient shared signal to measure both the x and y coordinates will depend on the electronic noise and the feature size of the anode pattern. A 250-μm-diameter charge cloud is shown projected on two expanded unit cell anode patterns of detectors featuring different pad and gap sizes to illustrate how small feature size will improve the charge sharing (Fig. 9). We anticipate that our first prototype detectors will feature 100-μm pads and gaps and that the effective threshold will be $\sim$150 keV. A 50-keV threshold should be possible if manufacturers can fabricate and bond detectors with 20-μm pads and gaps, the goal with eV Products' bonding technology development effort.

C. Demonstration of Imaging Using Charge Sharing

A laboratory demonstration of 3-D imaging in a charge-sharing configuration was conducted using a prototype detector of the earlier design (Fig. 1). The detector was operated in a modified bias and signal-processing configuration for this demonstration. The pixel rows and the strip columns were identically biased for electron collection. The row and column shaping amplifiers were identically set for gain, shaping time, and polarity. A collimated beam (200-μm diameter) of photons from a ^{57}Co source, incident on the cathode surface ($z = 0$), was directed at the center of a unit cell, the 200-μm pixel row contact pad. The cathode signal was used to trigger acquisition of event data. The largest signal for most events was recorded on the pixel row corresponding to the beam spot location.

The image of this beam spot (Fig. 10) was formed using events for which at least 10% of the signal was registered on a strip column electrode. This was 46% of the total number of triggered events. The event location (x, y) was determined for each event by the weighted average of the row and column signals. The z coordinate for each event was computed using the ratio of the cathode to anode sum pulse heights. The sum of row and column pulse heights was used to make the energy measurement. The measured energy resolution (FWHM) at 122 keV was 9.9 keV.

This imaging and spectroscopy capability is possible because a significant portion of the charge signal is shared across the 200-μm gap that separates the pixel row from the surrounding strip column electrode. It represents a feasibility demonstration of the charge-sharing strip detector design concept for anodes having 200-μm feature sizes.

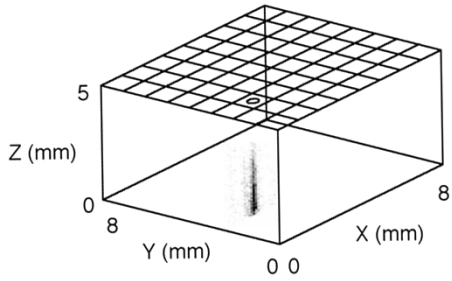

Fig. 10. Image of collimated beam of 122-keV photons formed using row and column charge sharing.

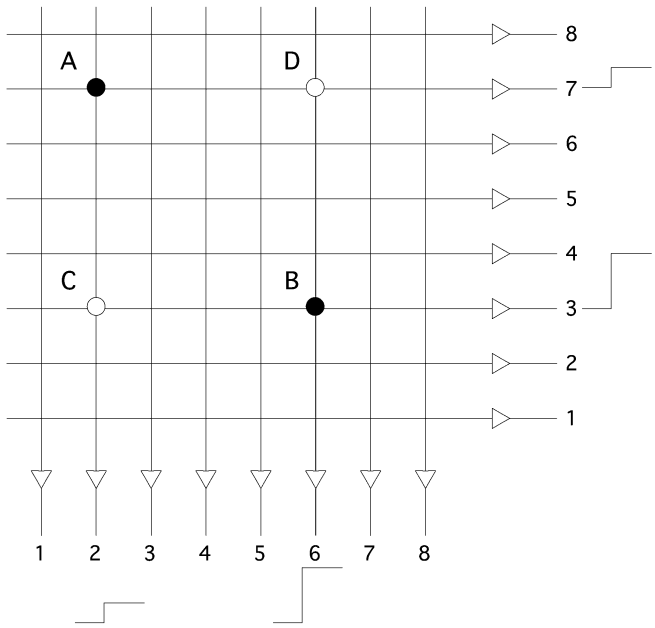

Fig. 11. Illustration of how 50:50 charge sharing and pulse-height measurements can resolve multihit ambiguity.

D. Resolving Multi-Hit Events

The ambiguity associated with identifying the true locations of multiple Compton interactions (multihits) in strip detectors is illustrated in Fig. 11. In this example, interactions at points A and B could be interpreted as having occurred at C and D unless there is some mechanism to associate the row with the column for each hit. Independent measurements of the arrival time of both column and row signals can be effective unless the interactions occur at the same depth (Z). If, however, feature sizes can be made small enough to achieve 50:50 row:column charge sharing, pulse height information can be used to eliminate this ambiguity. A and B would be identified as the true locations in this example as column, row (2, 7) and (6, 3) record the same pulse height.

VII. Charge-Sharing Strip Detector Simulations

Simulations of the single-sided charge-sharing strip detector (Fig. 2) were conducted at the University of Montreal. The potential across a 1-mm-wide unit cell under the first millimeter of a 10-mm-thick detector is shown in the top of Fig. 12. The anode pad bias is 1175 V. The grid bias is 1150 V. On the bottom is the weighting potential of one of the rows or columns. These plots

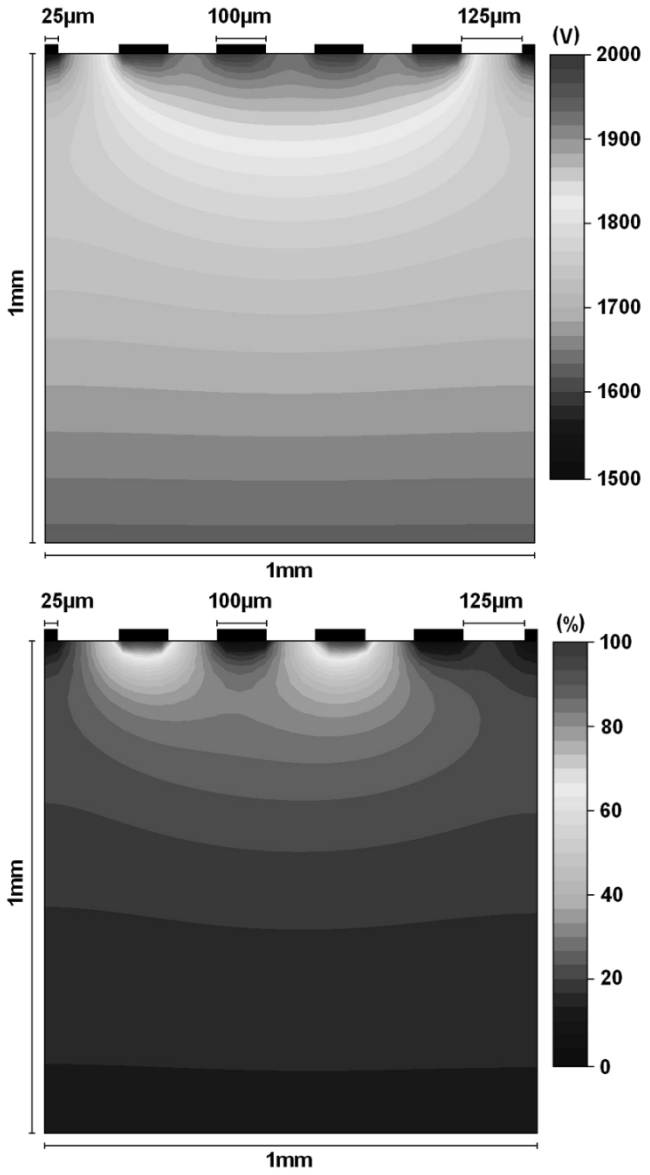

Fig. 12. Simulation of a 10-mm-wide unit cell for the first millimeter near the anode of a 10-mm-thick detector. Potential of unit cell (top). Weighting potential of one row or column (bottom).

indicate uniform fields in the bulk, the focusing effect of the grid electrode and that the advantages of the small pixel effect apply in this case. Simulated detector signals at various interaction depths (Fig. 13) from the charge transport and signal generation simulation are shown for one row or column (top) and for the depth sensing grid (bottom). The pulse height of signals is shown as a percentage of the unit charge deposited.

The simulation assumes 50:50 sharing between rows and columns of the charge signal reaching the anode surface. The simulation of row or column signals indicates little need for a depth of interaction correction of the energy measurement. The simulation of the depth sensing grid signal suggests that application of a long shaping time will be effective in establishing a measure of the depth of interaction independent of the cathode signal. Shaping times of 2 and 8 μs were simulated for the depth sensing grid signals at various interaction depths (Fig. 14). A signal-to-noise trade study is required to find an optimized

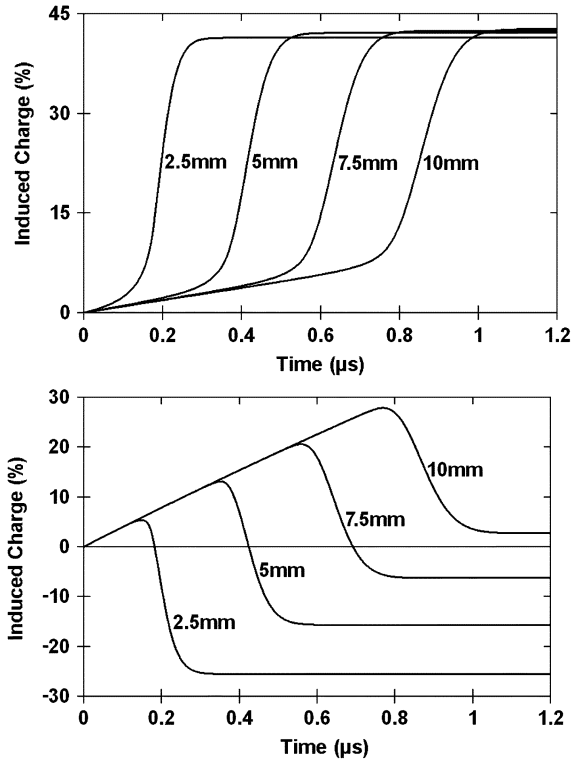

Fig. 13. Detector signals, as a percentage of total charge at various depths. Row or column signals (top). Depth sensing grid signals (bottom).

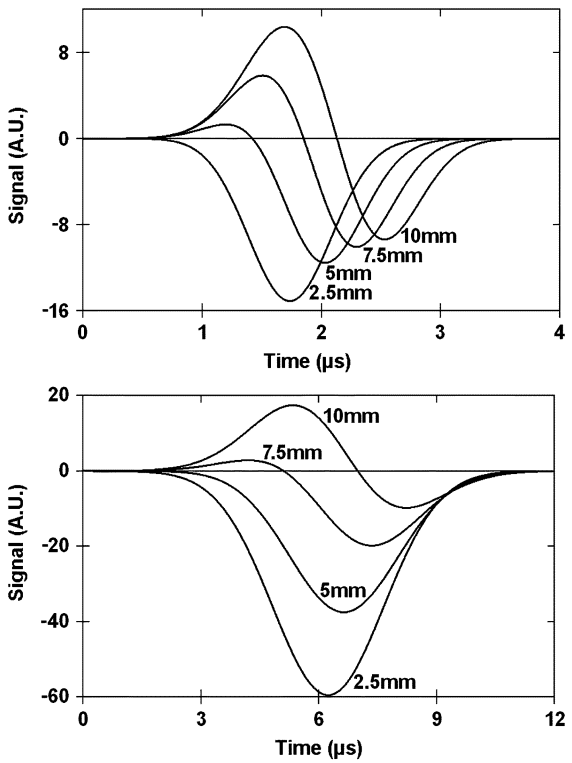

Fig. 14. Simulated depth sensing grid signals, relative units: 2 μs shaping (top); 8 μs (bottom).

solution. The capibility to determine interaction depth without the cathode signal is an advantage in closely packed arrays.

VIII. Conclusion and Future Work

Our goal is to develop and demonstrate mature designs for compact, efficient, high-performance CZT strip detectors for imaging and spectroscopy in the 0.05–1-MeV energy range and be ready to employ them in large-area detector arrays when large volumes of suitable CZT material with uniform properties become available and affordable. With this goal in mind, we are developing two single-sided strip detector designs.

We have demonstrated good spectroscopic, imaging and, now, detection efficiency performance with a prototype 5-mm-thick *orthogonal coplanar anode strip detector* and identified several factors that limit its performance. Good fabrication process control is required to achieve uniform response. While a reasonable approach employing 200-ns shaping has been demonstrated, implementation of the front-end electronics for processing the noncollecting strip column signal as an ASIC remains a concern.

We have introduced a new detector design, the single-sided *charge-sharing strip detector*, that will have a more straight-forward electronics implementation. In addition, the peformance of detectors employing this approach will improve with anode feature size technology.

References

[1] M. L. McConnell, J. R. Macri, J. M. Ryan, K. Larson, L.-A. Hamel, G. Bernard, C. Pomerleau, O. Tousignant, J.-C. Leroux, and V. Jordanov, "Three-dimensional imaging and detection efficiency performance of orthogonal coplanar CZT strip detectors," *Proc. SPIE*, vol. 4141, pp. 157–167, 2000.

[2] V. T. Jordanov, J. R. Macri, J. E. Clayton, and K. A. Larson, "Multi-electrode CZT detector packaging using polymer flip chip bonding," *Nucl. Instrum. Methods*, vol. A458, pp. 511–517, 2001.

[3] J. R. Macri, B. Dönmez, L.-A. Hamel, M. Julien, M. McClish, M. L. McConnell, R. S. Miller, J. M. Ryan, and M. Widholm, "Readout and performance of thick CZT strip detectors with orthogonal coplanar anodes," presented at the IEEE Nuclear Science Symp. Medical Imaging Conf., Norfolk, VA, 2002.

[4] P. N. Luke, "Unipolar charge sensing withh coplanar electrodes—Application to semiconductor detectors," *IEEE Trans. Nucl. Sci.*, vol. 42, pp. 207–213, 1995.

[5] E. Kalemci and J. L. Matteson, "Investigation of charge sharing among electrode strips for a CdZnTe detector," *Nucl. Instrum. Methods*, vol. A478, pp. 527–537, 2002.

[6] NIST: Physical Reference Data [Online]. Available: http://www.physics.nist.gov/PhysRefData/Star/Text/ESTAR.html